

Two-Center Interference in the Photoionization Delays of Kr₂


Saijoscha Heck¹, Meng Han^{1,*}, Denis Jelovina¹, Jia-Bao Ji¹, Conaill Perry¹, Xiaochun Gong²,
Robert Lucchese³, Kiyoshi Ueda^{1,4} and Hans Jakob Wörner^{1,†}

¹Laboratorium für Physikalische Chemie, ETH Zürich, 8093 Zürich, Switzerland

²State Key Laboratory of Precision Spectroscopy, East China Normal University, 200241 Shanghai, China

³Lawrence Berkeley National Laboratory, Berkeley, California 94720, USA

⁴Department of Chemistry, Tohoku University, Sendai, 980-8578, Japan

 (Received 25 January 2022; revised 22 April 2022; accepted 17 August 2022; published 21 September 2022)

We present the experimental observation of two-center interference in the ionization time delays of Kr₂. Using attosecond electron-ion-coincidence spectroscopy, we simultaneously measure the photoionization delays of krypton monomer and dimer. The relative time delay is found to oscillate as a function of the electron kinetic energy, an effect that is traced back to constructive and destructive interference of the photoelectron wave packets that are emitted or scattered from the two atomic centers. Our interpretation of the experimental results is supported by solving the time-independent Schrödinger equation of a 1D double-well potential, as well as coupled-channel multiconfigurational quantum-scattering calculations of Kr₂. This work opens the door to the study of a broad class of quantum-interference effects in photoionization delays and demonstrates the potential of attosecond coincidence spectroscopy for studying weakly bound systems.

DOI: 10.1103/PhysRevLett.129.133002

Two-center interference is one of the most prominent manifestations of the wave character of matter. The simplest demonstration consists of a double slit as first done in 1801 by Thomas Young with light waves [1] and in 1961 by Claus Jönsson with electrons [2]. Soon after that, it was noted by Cohen and Fano [3] that the electron wave from photoionization of diatomic molecules resembles the one behind the double slit. Since then, there have been numerous investigations of the molecular double slit in diatomic molecules [4–13]. The interference can be simply described with the superposition of two spherical waves departing from each atom of a diatomic molecule:

$$\Psi_{1,2} = \frac{1}{|r|} \cdot e^{i(k(r \pm R/2) + \Phi)}, \quad (1)$$

with an internuclear distance R , momentum k , and initial phase shift Φ [14]. So far, most of the experiments have studied the photoionization cross section of unaligned [3,4] and aligned [6,7,9,11,13,15] diatomic molecules. More recently the influence of two-center interference on high-harmonic generation was investigated in CO₂, N₂O [5,16–19] and H₂ [8,20].

Owing to the fact that photoionization delays are indeed closely linked with the variation in the cross section [21], it is expected that two-center interference also has a significant impact on the ionization dynamics in the time domain. Vladislav Serov and others made several pioneering predictions of such effects [22–28] on H₂ and H₂⁺ molecules. However, until now there has been no experimental

observation of the influence of the two-center interference on the photoionization delays. Here, we report the photoionization delay of the krypton dimer relative to its monomer and observe oscillations in the delay that can be traced back to the interference of the electron wave packets that are emitted or scattered from the two weakly bound atoms in Kr₂.

The experiment was performed by combining an XUV attosecond pulse train (APT) generated via high-harmonic generation in a 3 mm long gas cell filled with 20 mbar of xenon, covering the odd-order harmonics from H9 to H21, with an electron-ion coincidence spectrometer. The APT is focused into a cold krypton gas beam, which is produced via supersonic expansion, where it is spatially and temporally overlapped with a near-infrared (NIR) pulse of co-linear polarization. The APT and NIR pulses are phase locked in an actively stabilized Mach-Zehnder interferometer and their delay is controlled with a piezoelectric translation stage. Upon photoionization, the electrons and ions are detected in coincidence using COLd Target Recoil Ion Momentum Spectroscopy [29,30], which measures the three-dimensional momentum vectors of electrons and ions. A more detailed account of the experimental apparatus can be found in [31]. The photoelectron spectra of Kr and Kr₂ are measured simultaneously for XUV-NIR delays between 0 to 7 fs, using the reconstruction of attosecond beating by two-photon transitions (RABBIT) technique [32–35]. In RABBIT the intensity of the sidebands, which are the photoelectron bands generated by the additional absorption or emission of a single NIR photon

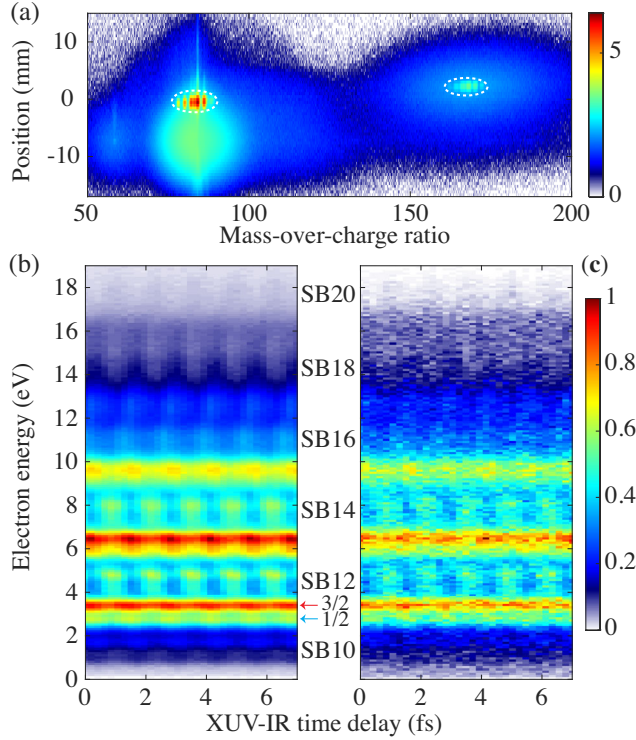


FIG. 1. (a) Measured ionic distribution as a function of the mass-over-charge ratio and the hit position on the detector along the direction of the supersonic molecular beam. The counts are shown on a logarithmic scale and displayed in false color. (b),(c) RABBIT spectrograms for electrons detected in coincidence with undissociated Kr^+ and Kr_2^+ , corresponding to the sharp distributions labeled with dashed ellipses in (a), respectively. Counts are normalized and shown in false color. In (b), the red and green arrows indicate the energy positions ionized by harmonic 11 for the two spin-orbit-coupling split states $^2P_{3/2}$ and $^2P_{1/2}$ of Kr_2^+ , respectively.

by a photoelectron, oscillates as a function of the XUV-NIR delay τ as

$$I_{\text{SB}} = B + A \cos(2\omega_{\text{NIR}}\tau - \Phi_{\text{XUV}} - \Phi_{\text{sys}}), \quad (2)$$

where A and B are constants, ω_{NIR} is the center frequency of NIR, Φ_{XUV} is the spectral phase difference between the two adjacent harmonic orders (which characterizes the attochirp), and Φ_{sys} is the system-specific phase term. The latter is what we are interested in.

In Fig. 1(a), we illustrate the measured ionic distribution as a function of the mass-over-charge ratio and the hit position on the detector. The sharp distributions of Kr^+ and Kr_2^+ [see dashed ellipses in Fig. 1(a)] indicate that these ions are from the undissociated channel, and their surrounding diffuse distributions of ions originate from the dissociative ionization channels of the larger clusters due to the kinetic-energy release in fragmentation. Figures 1(b) and 1(c) show the RABBIT spectrograms for photoelectrons

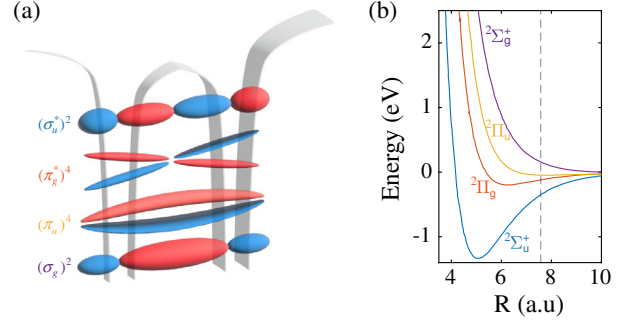


FIG. 2. Schematic illustration of the outermost valence molecular orbitals (a) for Kr_2 and the corresponding potential energy curves (b) for Kr_2^+ . In (b), the data is taken from Ref. [37] and the vertical dashed line indicates the equilibrium internuclear distance (7.578 a.u.) for the ground state of neutral Kr_2 . Spin-orbit coupling has been neglected for clarity.

measured in coincidence with the undissociated Kr^+ and Kr_2^+ , respectively. The photoelectrons were detected for an emission cone angle of $\theta_{\text{Lab}} = 0-25^\circ$ between the electron momentum vector and the XUV polarization, where the molecular axis with respect to the XUV polarization is randomly oriented. Six sidebands ranging from SB10 to SB20 can clearly be seen in both spectra, as labeled. There is also the signature of the spin-orbit coupling, which can be observed in Kr [36], as well as in Kr_2 [see the arrows in Fig. 1(b) and the matching signals in Fig. 1(c)]. In the analysis of the sideband oscillations, the energy range of each sideband was chosen to include both spin-orbit states. Because of the direct comparison of the same sidebands of Kr and Kr_2 , the XUV spectral phase Φ_{XUV} cancels out and the relative photoionization delays are determined by

$$\Delta\tau_{\text{Kr}_2-\text{Kr}} \simeq \hbar \frac{\Phi_{\text{sys}}^{\text{Kr}_2} - \Phi_{\text{sys}}^{\text{Kr}}}{\Delta E}, \quad (3)$$

where $\Delta E = 2\hbar\omega_{\text{NIR}}$ is the energy gap between two adjacent harmonic orders. The most fundamental difference between monomer and dimer is that the two-center potential of the dimer will cause additional effects on its photoionization delay.

In Kr_2 , the configuration of the outermost valence electrons is $(\sigma_g)^2(\pi_u)^4(\pi_g^*)^4(\sigma_u^*)^2$. The removal of one electron from one of these four molecular orbitals gives rise to the ionic states of $^2\Sigma_g^+$, $^2\Pi_u$, $^2\Pi_g$, and $^2\Sigma_u^+$, respectively, which are graphically illustrated in Fig. 2(a). The different ionic states will have different nuclear dynamics after photoionization, resulting in different fragments. In Fig. 2(b), we show the potential energy curves of the four ionic states as a function of the internuclear distance. $^2\Pi_g$ and $^2\Sigma_u^+$ states (corresponding to ionization of the antibonding orbitals) have a potential well, allowing the Kr_2^+ to remain bound. Thus, our experimental coincidence

measurements, performed with the undissociated Kr_2^+ , rule out the contributions from the other two states (${}^2\Pi_u^+$ and ${}^2\Sigma_g$). In spite of this important simplification, one still needs to consider two ionic states of opposite parities. The parity of the molecular orbital controls the initial phase difference between the emitted electron wave packets from the two centers. The gerade orbital launches wave packets with a equal initial phase, whereas the wave packets released from the two centers in the ungerade orbital have an initial π phase shift.

To demonstrate the parity effect in two-center interference on the photoionization delays, we first resort to a simple and intuitive model, i.e., we numerically solve the time-independent Schrödinger equation for a 1D model potential with parameters chosen to closely resemble Kr_2 . We used the double-well potential

$$V(x) = V(x, -R) + V(x, R), \quad (4)$$

where $R = 7.578$ a.u. and the potential shape is given by

$$V(x, x_0) = V_1 \frac{e^{-\frac{|x-x_0|}{\lambda}}}{\sqrt{(x-x_0)^2 + s^2}}, \quad (5)$$

with $s = 1$ a.u., $V_1 = -2.25$ a.u., and $\lambda = 3$ a.u. The ground state (gerade) and the first excited state (ungerade) of this double-well potential can be regarded as the molecular orbitals constructed by linear combination of two atomic s orbitals, just like the case of H_2 . The second (gerade) and third (ungerade) excited states are in analogy to the molecular orbitals constructed by two atomic p orbitals, where the π symmetry cannot be simulated by a 1D model. Therefore, in our calculations we use the second and third excited states as the initial states, and the choice of potential parameters (s, V_1, λ) gives the correct ionization potential ($I_p = 14.0$ eV) for the second excited state compared with the I_p of Kr. In Fig. 3(c), we illustrate the used double-well potential and the two normalized initial-state wave functions in coordinate space. Within time-independent perturbation theory, the electric-dipole transition matrix element is $\langle \psi_i | \hat{d} | \psi_f \rangle$, where ψ_i is the initial state and ψ_f is the final continuum state. The operator $\hat{d} = \hat{r}$ is the dipole operator in the length gauge. Here, we only consider dipole transitions in which the initial and final states have opposite parities. The photoionization cross section is then given by

$$\sigma = \frac{4\pi^2\omega}{3c} |\langle \psi_i | \hat{d} | \psi_f \rangle|^2, \quad (6)$$

shown in Fig. 3(a), where ω is the photon frequency and c is the speed of light. The energy derivative of the phase shift (argument of transition matrix element)

$$\tau_{\text{Wigner}} = \hbar \frac{\partial \arg(\langle \psi_i | \hat{d} | \psi_f \rangle)}{\partial E} \quad (7)$$

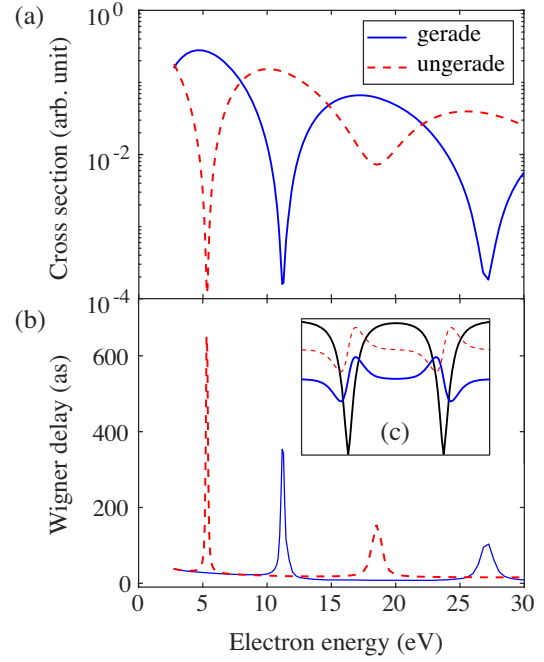


FIG. 3. (a) Photoionization cross section of the 1D system calculated with Eq. (6). (b) Corresponding Wigner delay calculated with Eq. (7). (c) Potential used in the calculations (black line) with the initial-state wave functions (blue and red lines). The ionization energies of the two states are 14.0 eV and 13.06 eV, respectively, and their vertical separation is added arbitrarily for clarity.

gives the photoionization time delay shown in Fig. 3(b). In all panels, we use *gerade* (in blue) and *ungerade* (in red) labels according to the symmetry of the initial state.

For each initial state, we observe peaks in the time delay that correspond to pronounced minima in the cross section due to destructive interference. More importantly, the peaks in the cross section of the gerade state correspond to the minima of the ungerade state and vice versa, which demonstrates the initial π phase shift between the two cases. We note that here the effect of two-center interference can be observed below 20 eV due to the very large internuclear distance of krypton dimer. In contrast, for the tightly bound molecules such as H_2 the energy range should cover up to several hundreds electron volts [27], which is a challenge for experiments.

From the RABBIT spectrograms shown in Fig. 1, we have extracted the phases of yield oscillations for the six sidebands using energy gating, followed by Fourier transformation. The uncertainty of the extracted sideband phase for each species (Kr and Kr_2) was determined by the B-over-A method [38] and that of their relative time delay was accordingly determined by the error propagation formula. In the Supplemental Material (SM) [39], we illustrate the details of data analysis. Figure 4(a) displays the extracted relative ionization delays $\Delta\tau_{\text{Kr}_2-\text{Kr}}$ between Kr_2 and Kr as a function of the sideband order or electron kinetic energy.

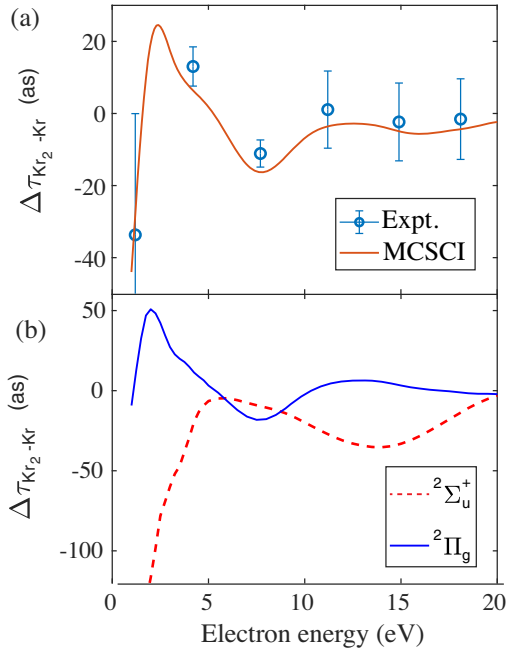


FIG. 4. (a) Ionization delays $\Delta\tau_{\text{Kr}_2-\text{Kr}}$ from experimental data (open circles), where values show the phase differences extracted from Figs. 1(b), 1(c) and the error bars represent the uncertainty of the phase extraction. The relative ionization delays from the MCSCI calculations are shown as a solid line. Theory for Kr_2 includes the cross-section weighted delays for the two bound states of Kr_2^+ , i.e., $^2\Sigma_u^+$ and $^2\Pi_g$. (b) State-resolved relative delays from the MCSCI calculations for the $^2\Sigma_u^+$ and $^2\Pi_g$ states. Note that the solid line in (a) is the cross-section-weighted average of the state-resolved delays in (b). For both experiment and theory the electron emission angles range from $\Theta_{\text{Lab}} = 0\text{--}25^\circ$ with respect to the XUV polarization, and the average over the molecular axis orientation in the lab frame is included in the calculations.

The oscillation of the relative ionization delay around 0 as can clearly be seen. The amplitude of the oscillation is gradually damped with increasing electron kinetic energy.

We further performed state-of-the-art photoionization calculations and extracted the photoionization delays for Kr_2 and Kr . The cross-section-weighted relative delay $\Delta\tau_{\text{Kr}_2-\text{Kr}}$ is shown and compared with the experimental results in Fig. 4(a), where good agreement between theory and experiment is achieved. These photoionization calculations were performed using the multichannel Schwinger configuration interaction (MCSCI) method [40,41] to obtain the photoionization matrix elements and the formalism outlined in [42] to obtain the photoionization delays. Here, we used a single-center expansion with $l_{\text{max}} = 200$ to represent all bound and continuum functions. The initial bound state was the Hartree-Fock state computed using a correlation-consistent polarized valence triple zeta basis set [43] using MOLPRO [44]. The ion states were then the frozen-core states created by removing one electron from the 4p orbitals. These four ionic states were all included in a close-coupling calculation and only the

results of $^2\Sigma_u^+$ and $^2\Pi_g$ state were extracted and displayed. All calculations were computed with a fixed internuclear distance of 7.578 a.u. (i.e., 4.01 Å) [45].

The state-resolved relative ionization delays for $^2\Sigma_u^+$ and $^2\Pi_g$ states, that give rise to the undissociated dimer, are shown in Fig. 4(b). Each of them oscillates with the electron energy and between them the anticyclic behavior can clearly be observed. Interestingly, the peak positions of the delays from gerade and ungerade wave functions roughly coincide with the peak positions resulting from the 1D time-independent Schrödinger equation calculation, which is a further indication that two-center interference is the cause for the oscillations observed in theory and experiment. Further, we see that the averaged relative ionization delays in Fig. 4(a) are dominated by the delays of the $^2\Pi_g$ state. The photoionization cross sections of $^2\Sigma_u^+$ and $^2\Pi_g$ are shown in the SM [39]. The cross section of $^2\Pi_g$ is 2 to 4 times larger than that of $^2\Sigma_u^+$. This is partially due to the fact that there are two degenerated $^2\Pi_g$ states with $\Lambda = +1$ and -1 for the orbital-angular-momentum projection quantum number that need to be summed over for the cross section. As a result of the different cross sections, the interference from gerade and ungerade wave functions does not cancel out completely, which results in an observable oscillation in the relative ionization delay. We note that the photoionization cross sections also display anticyclic oscillations in their amplitude (see SM [39]), which match the oscillations in the state-resolved delays displayed in Fig. 4(b). Comparing these accurate calculations to the solution of the time-independent Schrödinger equation of our 1D model potential, we conclude that the oscillations observed in the experiment and predicted by the MCSCI calculations are being caused by the interference of electron wave packets departing or scattering from the two atoms in Kr_2 . The large positive and negative delays in the energy range below ~ 5 eV, in experiment and theory in Fig. 4, may suggest that two-center interference between the photoelectron wave departing from one site and the diffracted wave from the other site contributes significantly to the enhancement of the time delays. To evaluate the contribution from this diffraction effect, additional MCSCI calculations have been carried out with initial states localized to a single Kr atom, in which case the photoelectron is emitted from one Kr atom only and is being diffracted from the other Kr atom: the calculated time delays (not shown) are almost identical to the results in Fig. 4(b), confirming that the observed oscillatory structure in the time delay mainly comes from the two center interference between the photoelectron wave emitted from one Kr atom and the diffracted wave from the other Kr atom.

In conclusion, we have demonstrated the manifestations of two-center quantum interference in the ionization time delays of a diatomic homonuclear molecule. We have done so in a fundamental theoretical manner by solving the time-independent Schrödinger equation of a 1D double-well

potential and experimentally by measuring the relative ionization delays between Kr and Kr₂, where the measurement result is quantitatively supported by state-of-the-art quantum-scattering calculations. These results show that two-center interference effects can be observed in attosecond photoionization delays. Such effects can be expected to be observed in many other systems as well, provided that the internuclear separation is sufficiently large or the electron-kinetic energy is sufficiently high, to fulfill the interference condition. Our results also show that the opposite modulations of initial states of opposite parity tend to cancel the signatures of two-center interference, which explains why the observed effects are relatively small. In cases where the energy intervals corresponding to ionization from initial states of different parity are resolvable, correspondingly larger effects can be expected. This is the case, in particular, in lighter diatomic molecules with shorter internuclear separations. However, two-center-interference effects can also be expected in larger systems consisting of two identical subunits, such as biphenyl and its derivatives or two-center metal complexes, be it in the gas or liquid phase [46]. Our results therefore pave the way to the investigation of a broad variety of quantum-interference effects in attosecond chronoscopy.

We thank A. Schneider and M. Seiler for their technical support. We gratefully acknowledge funding from the Swiss National Science Foundation (SNSF) through Projects No. 206021_170775 and No. 200021_172946, as well as ERC Project No. 772797. Work by M. H. and D. J. was supported by European Union's Horizon 2020 program under MCSA Grant No. 801459, FP-RESOMUS. Work by R. R. L. was supported by the U.S. Department of Energy (DOE), Office of Science, Basic Energy Sciences (BES) under Contract DE-AC02-05CH1123.

*Corresponding author.
menhan@ethz.ch

†Corresponding author.
hwoerner@ethz.ch

- [1] T. Young, The bakerian lecture. Experiments and calculations relative to physical optics, *Phil. Trans. R. Soc. London* **94**, 1 (1804).
- [2] C. Jönsson, Elektroneninterferenzen an mehreren künstlich hergestellten Feinspalten, *Z. Phys.* **161**, 454 (1961).
- [3] H. D. Cohen and U. Fano, Interference in the photoionization of molecules, *Phys. Rev.* **150**, 30 (1966).
- [4] X.-J. Liu, N. A. Cherepkov, S. K. Semenov, V. Kimberg, F. Gel'mukhanov, G. Prümper, T. Lischke, T. Tanaka, M. Hoshino, H. Tanaka *et al.*, Young's double-slit experiment using core-level photoemission from N₂: Revisiting Cohen-Fano's two-centre interference phenomenon, *J. Phys. B* **39**, 4801 (2006).
- [5] A. T. Le, X. M. Tong, and C. D. Lin, Evidence of two-center interference in high-order harmonic generation from CO₂, *Phys. Rev. A* **73**, 041402(R) (2006).
- [6] D. Akoury, K. Kreidi, T. Jahnke, T. Weber, A. Staudte, M. Schöffler, N. Neumann, J. Titze, L. P. H. Schmidt, A. Czasch, O. Jagutzki, R. A. C. Fraga, R. E. Grisenti, R. D. Muiño, N. A. Cherepkov, S. K. Semenov, P. Ranitovic, C. L. Cocke, T. Osipov, H. Adaniya, J. C. Thompson, M. H. Prior, A. Belkacem, A. L. Landers, H. Schmidt-Böcking, and R. Dörner, The simplest double slit: Interference and entanglement in double photoionization of H₂, *Science* **318**, 949 (2007).
- [7] M. S. Schöffler *et al.*, Photo-double-ionization of H₂: Two-center interference and its dependence on the internuclear distance, *Phys. Rev. A* **78**, 013414 (2008).
- [8] S. Baker, J. S. Robinson, M. Lein, C. C. Chirila, R. Torres, H. C. Bandulet, D. Comtois, J. C. Kieffer, D. M. Villeneuve, J. W. G. Tisch, and J. P. Marangos, Dynamic Two-Center Interference in High-Order Harmonic Generation from Molecules with Attosecond Nuclear Motion, *Phys. Rev. Lett.* **101**, 053901 (2008).
- [9] K. Kreidi *et al.*, Interference in the Collective Electron Momentum in Double Photoionization of H₂, *Phys. Rev. Lett.* **100**, 133005 (2008).
- [10] Y. J. Chen and J. Liu, High-order harmonic generation from diatomic molecules with large internuclear distance: The effect of two-center interference, *Phys. Rev. A* **77**, 013410 (2008).
- [11] L. R. Hargreaves, C. Colyer, M. A. Stevenson, B. Lohmann, O. Al-Hagan, D. H. Madison, and C. G. Ning, (2,2e) study of two-center interference effects in the ionization of N₂, *Phys. Rev. A* **80**, 062704 (2009).
- [12] H. Chaluvadi, Z. N. Ozer, M. Dogan, C. Ning, J. Colgan, and D. Madison, Observation of two-center interference effects for electron impact ionization of N₂, *J. Phys. B* **48**, 155203 (2015).
- [13] X. Li, X. Ren, K. Hossen, E. Wang, X. Chen, and A. Dorn, Two-center interference in electron-impact ionization of molecular hydrogen, *Phys. Rev. A* **97**, 022706 (2018).
- [14] M. Kunitski, N. Eicke, P. Huber, J. Köhler, S. Zeller, J. Voigtsberger, N. Schlott, K. Henrichs, H. Sann, F. Trinter, L. P. H. Schmidt, A. Kalinin, M. S. Schöffler, T. Jahnke, M. Lein, and R. Dörner, Double-slit photoelectron interference in strong-field ionization of the neon dimer, *Nat. Commun.* **10**, 1 (2019).
- [15] L. Nagy, S. Borbély, and K. Póra, Interference effects in the photoionization of molecular hydrogen, *Phys. Lett. A* **327**, 481 (2004).
- [16] T. Kanai, S. Minemoto, and H. Sakai, Quantum interference during high-order harmonic generation from aligned molecules, *Nature (London)* **435**, 470 (2005).
- [17] C. Vozzi, F. Calegari, E. Benedetti, J. P. Caumes, G. Sansone, S. Stagira, M. Nisoli, R. Torres, E. Heesel, N. Kajumba, J. P. Marangos, C. Altucci, and R. Velotta, Controlling Two-Center Interference in Molecular High Harmonic Generation, *Phys. Rev. Lett.* **95**, 153902 (2005).
- [18] A. Rupenyan, P. M. Kraus, J. Schneider, and H. J. Wörner, High-harmonic spectroscopy of isoelectronic molecules: Wavelength scaling of electronic-structure and multielectron effects, *Phys. Rev. A* **87**, 033409 (2013).
- [19] A. Rupenyan, P. M. Kraus, J. Schneider, and H. J. Wörner, Quantum interference and multielectron effects in high-harmonic spectra of polar molecules, *Phys. Rev. A* **87**, 031401(R) (2013).

- [20] E. V. van der Zwan and M. Lein, Two-center interference and ellipticity in high-order harmonic generation from H_2^+ , *Phys. Rev. A* **82**, 033405 (2010).
- [21] J. M. Dahlström, D. Guénot, K. Klünder, M. Gisselbrecht, J. Mauritsson, A. L'Huillier, A. Maquet, and R. Taïeb, Theory of attosecond delays in laser-assisted photoionization, *Chem. Phys.* **414**, 53 (2013).
- [22] V. V. Serov, I. A. Ivanov, and A. S. Kheifets, Single-photon double ionization of H_2 away from equilibrium: A showcase of two-center electron interference, *Phys. Rev. A* **86**, 025401 (2012).
- [23] I. A. Ivanov, A. S. Kheifets, and V. V. Serov, Attosecond time-delay spectroscopy of the hydrogen molecule, *Phys. Rev. A* **86**, 063422 (2012).
- [24] V. V. Serov, V. L. Derbov, and T. A. Sergeeva, Interpretation of time delay in the ionization of two-center systems, *Phys. Rev. A* **87**, 063414 (2013).
- [25] V. V. Serov and A. S. Kheifets, p - h symmetry breaking in dissociative photoionization of H_2 due to the molecular ion interacting with the ejected electron, *Phys. Rev. A* **89**, 031402(R) (2014).
- [26] Y. Liao, Y. Zhou, L.-W. Pi, Q. Ke, J. Liang, Y. Zhao, M. Li, and P. Lu, Two-center interference and stereo Wigner time delay in photoionization of asymmetric molecules, *Phys. Rev. A* **104**, 013110 (2021).
- [27] Q.-C. Ning, L.-Y. Peng, S.-N. Song, W.-C. Jiang, S. Nagele, R. Pazourek, J. Burgdörfer, and Q. Gong, Attosecond streaking of Cohen-Fano interferences in the photoionization of H_2^+ , *Phys. Rev. A* **90**, 013423 (2014).
- [28] R. Pazourek, S. Nagele, and J. Burgdörfer, Attosecond chronoscopy of photoemission, *Rev. Mod. Phys.* **87**, 765 (2015).
- [29] J. Ullrich, R. Moshhammer, A. Dorn, R. Drner, L. P. H. Schmidt, and H. Schmidt-Böcking, Recoil-ion and electron momentum spectroscopy: Reaction-microscopes, *Rep. Prog. Phys.* **66**, 1463 (2003).
- [30] R. Dörner, V. Mergel, O. Jagutzki, L. Spielberger, J. Ullrich, R. Moshhammer, and H. Schmidt-Böcking, Cold target recoil ion momentum spectroscopy: A 'momentum microscope' to view atomic collision dynamics, *Phys. Rep.* **330**, 95 (2000).
- [31] S. Heck, D. Baykusheva, M. Han, J.-B. Ji, C. Perry, X. Gong, and H. J. Wörner, Attosecond interferometry of shape resonances in the recoil frame of CF_4 , *Sci. Adv.* **7**, eabj8121 (2021).
- [32] P. M. Paul, E. S. Toma, P. Breger, G. Mullot, F. Augé, P. Balcou, H. G. Muller, and P. Agostini, Observation of a train of attosecond pulses from high harmonic generation, *Science* **292**, 1689 (2001).
- [33] K. Klünder, J. M. Dahlström, M. Gisselbrecht, T. Fordell, M. Swoboda, D. Guénot, P. Johnsson, J. Caillat, J. Mauritsson, A. Maquet, R. Taïeb, and A. L'Huillier, Probing Single-Photon Ionization on the Attosecond Time Scale, *Phys. Rev. Lett.* **106**, 143002 (2011).
- [34] M. Huppert, I. Jordan, D. Baykusheva, A. von Conta, and H. J. Wörner, Attosecond Delays in Molecular Photoionization, *Phys. Rev. Lett.* **117**, 093001 (2016).
- [35] X. Gong, S. Heck, D. Jelovina, C. Perry, K. Zinchenko, R. Lucchese and H. J. Wörner, Attosecond spectroscopy of size-resolved water clusters, *Nature* (2022).
- [36] I. Jordan, M. Huppert, S. Pabst, A. S. Kheifets, D. Baykusheva, and H. J. Wörner, Spin-orbit delays in photoemission, *Phys. Rev. A* **95**, 013404 (2017).
- [37] R. Kalus, I. Paidarová, D. Hrivňák, P. Paška, and F. X. Gadéa, Modelling of Kr_n^+ clusters ($n = 2-20$). I. Structures and energetics, *Chem. Phys.* **294**, 141 (2003).
- [38] J.-B. Ji, S. Heck, M. Han, and H. J. Wörner, Quantitative uncertainty determination of phase retrieval in Rabbit, *Opt. Express* **29**, 27732 (2021).
- [39] See Supplemental Material at <http://link.aps.org/supplemental/10.1103/PhysRevLett.129.133002> for details on the data analysis and the state-resolved photoionization cross sections.
- [40] R. E. Stratmann and R. R. Lucchese, A graphical unitary group approach to study multiplet specific multichannel electron correlation effects in the photoionization of O_2 , *J. Chem. Phys.* **102**, 8493 (1995).
- [41] R. E. Stratmann, R. W. Zurales, and R. R. Lucchese, Multiplet-specific multichannel electron-correlation effects in the photoionization of NO, *J. Chem. Phys.* **104**, 8989 (1996).
- [42] D. Baykusheva and H. J. Wörner, Theory of attosecond delays in molecular photoionization, *J. Chem. Phys.* **146**, 124306 (2017).
- [43] A. K. Wilson, D. E. Woon, K. A. Peterson, and T. H. Dunning, Gaussian basis sets for use in correlated molecular calculations. IX. The atoms gallium through krypton, *J. Chem. Phys.* **110**, 7667 (1999).
- [44] H.-J. Werner, P. J. Knowles, G. Knizia, F. R. Manby, and M. Schütz, MOLPRO: A general-purpose quantum chemistry program package, *WIREs Comput. Mol. Sci.* **2**, 242 (2012).
- [45] J. A. Barker, R. O. Watts, J. K. Lee, T. P. Schafer, and Y. T. Lee, Interatomic potentials for krypton and xenon, *J. Chem. Phys.* **61**, 3081 (1974).
- [46] I. Jordan, M. Huppert, D. Rattenbacher, M. Peper, D. Jelovina, C. Perry, A. von Conta, A. Schild, and H. J. Wörner, Attosecond spectroscopy of liquid water, *Science* **369**, 974 (2020).